Phosphorylation Triggers Domain Separation in the DNA Binding Response Regulator NarL†

Jeffrey H. Zhang,[‡,§,||] Gaoping Xiao,[‡,⊥] Robert P. Gunsalus,*[,⊥,#] and Wayne L. Hubbell*[,§,||,#]

Jules Stein Eye Institute, Department of Chemistry and Biochemistry, Department of Microbiology, Immunology, and Molecular Genetics, and Molecular Biology Institute, University of California, Los Angeles, California 90095-1489

Received November 21, 2002

ABSTRACT: DNA binding proteins of two-component signal transduction systems in microorganisms are activated by phosphorylation through an unknown mechanism. NarL is an example from the nitrate/nitrite signal transduction system of *Eschericia coli*. NarL consists of N- and C-terminal domains, the latter of which contains the DNA binding elements. To explore the mechanism of activation, single nitroxide side chains were introduced, one at a time, at nine different sites throughout the C-terminal domain to monitor the tertiary structure and the status of the surface in contact with the N-terminal domain. In addition, three pairs of doubly labeled proteins were prepared to monitor the interdomain distance using the magnetic dipolar interaction. The results of these site-directed spin-labeling studies reveal that phosphorylation at a distant site in the N-terminal domain triggers domain separation, likely by a hinge-bending motion. This in turn presents key elements of the C-terminal domain for docking to the DNA target in the configuration described in the recent crystal structure. The data also imply that a single conformation of unphosphorylated NarL exists in solution, and there is no detectable equilibrium between the closed and open conformations.

Signal transduction in many types of microorganisms proceeds by means of phospho-relay circuits known as two-component regulatory systems (*1*, *2*). These systems are nearly universally distributed in the Bacteria and Archaea and occur in isolated cases in several eukaryotic organisms. They allow cells to monitor and respond to a variety of environmental and intracellular conditions including osmolarity, anaerobiosis, acid stress, and nutrient availability.

The Nar system of *Escherichia coli* is a paradigm of two-component regulatory systems. Nar is composed of four regulatory proteins: two receptors in the cell membrane (NarX and NarQ) and two cognate response regulatory proteins in the cytoplasm (NarL and NarP). These proteins modulate transcription of ∼25 genes needed for anaerobic respiration with nitrate or nitrite as electron acceptors (*3*). They also suppress the expression of another 15 genes involved in alternative respiratory pathways or in fermentation. In the presence of nitrate or nitrite, the receptor is activated, and the signal is relayed to the cognate regulator NarL or NarP via phosphorylation of a specific aspartic acid residue located at position 59. In turn, phosphorylation triggers a conformational switch in the response regulator that enables its interaction at Nar-regulated promoters to activate or repress transcription of the downstream genes. The molecular mechanism of this switch is the subject of the present study.

NarL and NarP, like most response regulators, consist of two domains (an N- and C-terminal domain). Other response regulators may have a single domain (e.g., CheY) or even three (NtrC). Despite these differences, regulation by phosphorylation is a common theme in all two-component regulatory systems, and a molecular description of the phosphorylation switch in the regulator proteins is thus central to understanding the signal transduction mechanism. To this end, efforts have been made to determine structures of both the unphosphorylated and phosphorylated states. Within the large family of response regulators, structures for the unphosphorylated forms of some regulators and phosphorylated forms of single-domain proteins and isolated domains of two- or three-domain proteins have been reported (CheY, Spo0A, NtrC, FixJ, and PhoB) (*4*−*8*). NarL is one of two response regulators, along with DrrD from *Thermotoga maritima*, with a resolved structure for the intact unphosphorylated full-length protein (*9*−*12*). However, the structure of a phosphorylated full-length response regulator has been elusive due to the short half-life of the activated species (*13*), and it has not been possible to explore the mechanism of the phosphorylation switch with crystallography.

On the other hand, recent studies using NMR have revealed that phosphorylation causes internal conformational changes in the isolated N-terminal receiver domain of NtrC (*14*). Similar changes are observed in crystal structures of isolated receiver domains in FixJ and SpoOA after phos-

† This work was supported in part by grants from the NIH [AI21678 (to R.P.G.) and EY05216 (to W.L.H.)], the Jules Stein Professor Endowment, and the Bruce Ford Bundy and Anne Smith Bundy Foundation (W.L.H.).

* To whom correspondence should be addressed.

‡ These authors contributed equally to this work.

§ Jules Stein Eye Institute.

|| Department of Chemistry and Biochemistry.

⊥ Department of Microbiology, Immunology, and Molecular Genetics.

Molecular Biology Institute.

10.1021/bi0272205 CCC: $25.00
Published on Web 02/14/2003

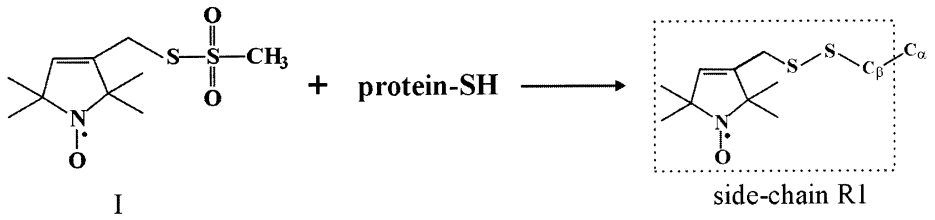

I

FIGURE 1: Reaction of methanethiosulfonate reagent (**I**) with a protein sulfhydryl group to generate the nitroxide side chain R1.

phorylation (*15*, *16*). In addition, SDSL[1] studies of full-length NtrC detected phosphorylation-induced structural changes that were interpreted as modulation of interdomain interactions, although specific interactions or conformational changes were not identified (*17*).

In the case of NarL, important clues to the mechanism have recently been uncovered. First is the fact that the isolated C-terminal domain ($NarL^C$) binds constitutively to DNA (*18*, *19*). Second, the crystal structure of a $NarL^C$/DNA complex reveals that $NarL^C$ retains the structure of the C-terminal domain in the whole molecule (*18*). Moreover, in the whole molecule the N-terminal domain occludes key residues of $NarL^C$ involved in DNA binding. These results suggest that the N-terminal domain of NarL masks the DNA binding region of the C-terminal domain, until phosphorylation triggers a change in conformation leading to separation of the domains (*10*). This model is of particular interest because the phosphorylation site in the N-terminal domain (D59) is far removed from the interdomain interface.

In the studies reported here, the SDSL method (for reviews see refs *20*−*23*) was used to explore phosphorylation-dependent structural changes in NarL. Single nitroxide side chains were placed at sites throughout the C-terminal domain to monitor both the internal structure and the status of the contact surface with the N-terminal domain. In addition, pairs of nitroxide side chains were placed across the interdomain interface, and the magnetic dipolar interaction between the spins was used to monitor interresidue distances. In the unphosphorylated state, the mobilities of the nitroxide side chains and the interresidue distances are consistent with the known crystal structure of NarL (*10*). Upon phosphorylation, changes in the mobilities of single nitroxide side chains and in the interresidue distances in the doubly labeled proteins are observed that suggest a separation of the N- and C-terminal domains, likely by a hinge-bending motion.

MATERIALS AND METHODS

Preparation of NarL Proteins. The wild-type and mutant NarL proteins and NarL domains were prepared as described previously (*19*). Cysteine substitution mutants were prepared using the Kunkel method with the M13MK1 *narL* template (*24*). The mutated genes were subcloned into plasmid pQE9, which adds a histidine tag at the N-terminus containing the sequence MRGSHHHHHGS. Fidelity of the cloned genes was confirmed by DNA sequencing (Laragen Inc., Los Angeles, CA). The wild-type NarL protein contains no cysteine residues.

Full-length NarL proteins and the isolated N-terminal (residues 2−144) and C-terminal (residues 147−216) NarL domains were produced in *E. coli* (strain JM109) cells and purified to at least 95% purity on a Pharmacia HiTrap Chelating HP column (1 mL). NarL was eluted with a gradient of buffer A (20 mM phosphate buffer, 10 mM imidazole, 1 M NaCl, pH 7.8) to buffer B (20 mM phosphate buffer, 500 mM imidazole, 0.1 M NaCl, pH 7.8). NarL elutes at ≈40% buffer B. Protein purity was examined using SDS−PAGE analysis on the Phast Gel System (Pharmacia) and stained with 0.25% w/v Coomassie Brilliant Blue. Loading buffer (1.25% SDS, 2.5% β-mercaptoethanol, 0.005% Bromophenol blue, 2.5 mM Tris, pH 8.0) was added to protein samples (1 μg) before being loaded on Phast gels.

Spin-Labeling and EPR Spectroscopy. Cysteine mutants of NarL were selectively spin-labeled with a 5-fold excess of (1-oxy-2,2,5,5-tetramethylpyrrolinyl-3-methyl)methanethiosulfonate (**I**) (kindly provided by Kálmán Hideg, University of Pécs, Hungary) in a buffer containing 50 mM MES, 300 mM NaCl, and 1 mM EDTA, pH 7.5. This reaction generates the nitroxide side chain designated R1 (Figure 1). Unreacted reagent was removed on a HiTrap desalting column (Pharmacia) eluting with 50 mM MES and 50 mM NaCl, pH 6.9. Samples were concentrated in a Microcon concentrator (3 kDa cutoff for $NarL^C$ 204R1 and 10 kDa cutoff for full-length NarL mutants; Millipore) to approximately 500 μM. Prior to EPR analysis, Ficoll (Sigma Chemicals), a nonionic polymer of sucrose, was added to a final concentration of 30% w/v to increase solution viscosity to approximately 3 cP. Assuming Stokes−Einstein behavior, this reduces the rotational correlation time of NarL to ≈20 ns. This is sufficiently long to have only minor effects on the resonance line shapes of nitroxides in the intermediate motional regime, and the EPR spectra thus reflect motion of the nitroxide relative to the protein.

Samples for EPR (≈5 μL) were contained in quartz capillaries, and spectra were recorded using a Varian E-109 spectrometer fitted with a 2-loop−1-gap resonator (Medical Advances, Milwaukee, WI). Incident microwave power was 2 mW, and modulation amplitude was optimized for maximum signal with no line shape distortion. For measurement of exchange rate with Ni(EDDA) (synthesized according to ref *25*) the concentration of Ni(EDDA) was 3 mM, and the samples were contained in TPX capillaries (Medical Advances, Milwaukee, WI). The power saturation method used to measure exchange rates is described in detail in Oh et al. (*26*). Distance measurements in doubly spin-labeled NarL were performed according to Altenbach et al. (*27*).

Phosphorylation of NarL. Spin-labeled NarL was phosphorylated by incubating 200 μM protein with 256 mM acetyl phosphate in buffer (50 mM MOPS, 50 mM KCl, 20 mM $MgCl_2$, pH 7.0) for 30 min at room temperature. The

[1] Abbreviations: EPR, electron paramagnetic resonance; MES, 2-(*N*-morpholino)ethanesulfonic acid; MOPS, 3-(*N*-morpholino)propanesulfonic acid; Ni(EDDA), nickel(II) ethylenediaminediacetate; SDSL, site-directed spin-labeling.

samples were then placed on ice for EPR analysis. Phosphorylation was routinely monitored on 20% w/v acrylamide native PAGE (Phast System, Pharmacia), where phosphorylated samples migrate slower than unphosphorylated NarL (S. Rech, M. Jarvis, and R. P. Gunsalus, personal communication). Protein samples (1.0 μg) for electrophoresis were loaded on Phast gels in loading buffer (10% glycerol, 50 mM Tris, pH 6.8, 10 mM EDTA, 0.005% Bromophenol blue). Proteins were visualized by staining with 0.25% w/v Coomassie Brilliant Blue.

Mass Spectrometry. Electrospray ionization mass spectrometry was employed to determine whether more than one site in NarL was phosphorylated by acetyl phosphate, to determine whether any acylation took place, and to estimate the extent of the spin-labeling reaction. For this purpose, NarL protein samples (20−40 μg) were made to 5% (v/v) acetonitrile and loaded onto a Protein MicroTrap (1 mm, Michrom BioResources), previously equilibrated in 0.1% trifluoroacetic acid in 5% acetonitrile, at a flow rate of 25 μL/min. The trap was developed with a linear gradient to 0.1% trifluoroacetic acid and 80% acetonitrile over 15 min, and the effluent was directed to the Ionspray source of a triple quadrupole electrospray ionization mass spectrometer (API III+; Applied Biosystems, Foster City, CA) operated in positive ion mode as described previously (*28*).

RESULTS

R1 Dynamics and Solution Structure of NarL. Using single cysteine substitution mutants and the chemistry of Figure 1, R1 side chains were introduced throughout the C-terminal domain of NarL, one at a time, at the positions shown in Figure 2. Spin-labeling efficiency, estimated by electrospray ionization mass spectrometry, was greater than 90%.

The mobility of the R1 side chain, reflected in the EPR spectrum, is determined by the secondary and supersecondary structure (*29*), backbone dynamics (*30*), and the type and degree of interactions made with the local environment (*31*). The R1 side chain thereby serves as a molecular "sensor" of local structure and dynamics and, most importantly, of changes in the secondary and tertiary structure related to function (*22*). The particular sites shown in Figure 2 were selected to monitor the state of each of the four α helices (α7−α10; residues 161, 169, 175, 196, 211), the connecting loop with the N-terminal domain (α6/α7; residue 157), the interhelical loops (α7/α8, α8/α9; residues 171, 181), and the interface between the N- and C-terminal domains (residue 204).

Figure 3 (black traces) shows the EPR spectra of R1 at all single sites in NarL investigated in this study. Residues 161R1, 169R1, 175R1, 196R1, and 211R1 are located at solvent-exposed helical surface sites in the crystal structure of NarL (Figure 1). R1 residues at such sites have been extensively investigated in the helical proteins T4L (*32*, *33*), diphtheria toxin T domain (*34*), colicin E1 (*35*), and annexin XII (*29*) and can be classified as either interacting or noninteracting with respect to R1 (*29*), depending on whether the nitroxide makes contacts with nearby residues in the structure.

At noninteracting helical surface sites, torsional oscillations of the bonds within the R1 side chain give rise to an anisotropic diffusion of the nitroxide ring. If fluctuations of

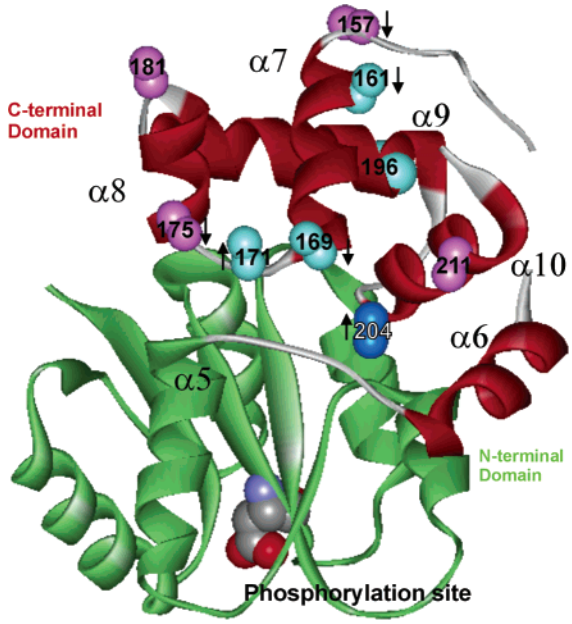

FIGURE 2: Crystal structure of unphosphorylated NarL (PDB file 1A04). The N- and C-terminal domains are in green and red, respectively. The phosphorylation site (D59) is shown as a space-filling model. Residues selected for spin-labeling are identified by spheres on the α and β carbon atoms (both atoms are shown to indicate the direction of the side chain). The spheres are colored according to the relative mobility of the nitroxide side chain in the unphosphorylated state, with violet being most mobile, blue as least mobile, and cyan an intermediate state. Arrows next to the spheres indicate an increase (up arrow) or decrease (down arrow) in mobility upon phosphorylation of NarL.

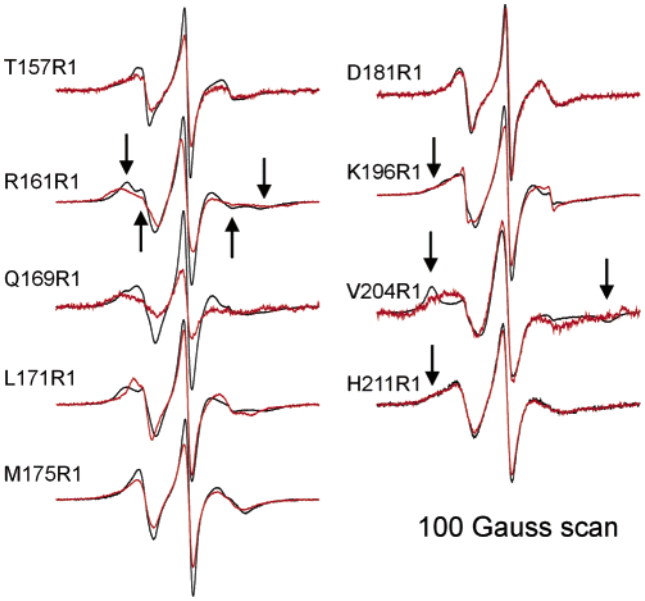

FIGURE 3: EPR spectra of spin-labeled full-length NarL mutants before (black trace) and after (red trace) phosphorylation at D59. Each spectrum was recorded for the protein in 30% w/v Ficoll to reduce the contribution of protein rotational diffusion to the side chain motion. Scan widths were 100 G, and spectra within each pair were normalized to the same number of spins. The arrows refer to features discussed in the text.

the helical backbone are of low amplitude, the anisotropic internal motion of the side chain dominates the overall dynamics, giving a distinctive EPR spectral line shape, illustrated by 161R1 in helix α7 (Figure 3) (*30*, *33*). The arrows in Figure 3 on the spectrum of 161R1 mark the

resolved outer (down arrows) and inner (up arrows) hyperfine extrema that characterize a single dynamic population of nitroxides with constrained anisotropic motion (*36*). The spectrum of 169R1 in the same helix suggests a similar motion for R1 at this site, although the hyperfine extrema are not as well resolved. These assignments as noninteracting helix surface sites are in good agreement with expectations based on the crystal structure.

In addition to the internal modes of the side chain discussed above, fluctuations of the polypeptide backbone contribute to the motion of the nitroxide. For noninteracting helix surface sites, backbone fluctuations with nanosecond correlation times of sufficient amplitude can result in more extensive averaging of the nitroxide magnetic parameters, resulting in a line shape more characteristic of isotropic than anisotropic motion. This is apparently the case for helix surface site 175R1, where hyperfine extrema are not resolved, and the line widths and overall spectral breadth are small compared to 161R1 and 169R1. This is consistent with the location of 175R1 at the N-terminus of α8, because backbone motions generally increase in amplitude toward the ends of helices (*32*).

The remaining helix surface residues 196R1 (in α9) and 211R1 (in α10) have more complex, multicomponent, EPR spectra, indicative of interactions of the nitroxide ring with the local environment. This is evident in the low-amplitude, broad spectral components in the wings that correspond to relatively immobilized nitroxides (marked by arrows in Figure 3 for 196R1 and 211R1). The origins of the interactions are unknown.

Residue 204R1 is located on α10 but is buried at the interface between the C- and N-terminal domains, with a fractional solvent accessibility for the native valine of only 6% in the crystal structure. An experimental value for the solvent accessibility of the R1 residue is provided by the collision rate of the nitroxide with the paramagnetic complex Ni(EDDA) in solution. The collision rate is expressed in terms of the proportional and dimensionless collision parameter Π (*25*). Consistent with a buried location for 204R1, Π[Ni(EDDA)] is 0.05. For comparison, R1 at buried sites in T4L range from 0.003 to 0.05, while fully solvent-exposed residues on helical surfaces range from 0.2 to 1 (C. Altenbach and W. L. Hubbell, unpublished observation). Moreover, the unique EPR spectrum for 204R1 is dominated by a strongly immobilized component characteristic of a buried residue, the outer hyperfine extrema of which are identified by arrows in Figure 3.

Residues 157R1, 171R1, and 181R1 are located in interhelical loops, and a wide range of dynamic modes has been observed for R1 at such sites, depending on the loop structure and local interactions of both the backbone and side chain (*29*, *32*, *35*). The loop residues in NarL are in keeping with this heterogeneous behavior. R1 at 157 has two spectral components corresponding to highly mobile and immobile populations of nitroxides (Figure 3). The existence of a highly mobile population implies a dynamic state for the C-terminal end of the long α6/α7 loop structure that links the C- and N-terminal domains (residues 141−157). Part of this loop (residues 143−149) was not resolved in the crystal structure due to disorder, suggesting a dynamic state for the entire linker in solution. For 171R1, the spectral line shape is similar to 161R1 and indicates an ordered, anisotropic nitroxide motion. This in turn implies an ordered backbone for the short α7/α8 interhelical loop. Finally, the sharp spectral features for 181R1 suggest a single state of high mobility for the nitroxide (note the narrow central line width).

Phosphorylation-Induced Changes in NarL Structure: Deductions from Changes in R1 Dynamics. Figure 3 shows the spectra of the various labeled mutants following phosphorylation of NarL at D59 in the N-terminal domain (red traces), superposed on the corresponding spectra of the unphosphorylated state. Remarkably, phosphorylation at a distant site produces changes in the EPR spectra, and hence mobility, for R1 side chains throughout the α7/α8 helical hairpin (sites 161, 169, 171, 175) and at site 204R1. The arrows in Figure 2 indicate the direction of mobility changes observed. In α7, both 161R1 and 169R1, at opposite ends of the helix, show similar decreases in mobility. In α8, 175R1 also has a decrease in mobility, while 171R1 in the α7/α8 loop has an increase in mobility. It should be emphasized that the EPR spectra for residues 161, 169, 171, and 175 in the phosphorylated state, although different from the unphosphorylated state, are still compatible with the basic tertiary fold of the C-terminal domain in the crystal structure. That is, the spectra of 161R1, 169R1, and 175R1 are still within the range observed for helix surface sites and 171 for loop sites. That a global change in the fold has not occurred is supported by the lack of spectral changes at 196R1 in α9, a helix involved in DNA binding (*18*), and at 211R1 in α10. Relatively small conformational changes of the α7/α8 helical hairpin within the C-terminal domain can account for the spectral changes (see Discussion).

On the other hand, the changes in the spectrum and solvent accessibility of 204R1 triggered by phosphorylation cannot be accounted for by a subtle conformational change but require a large-scale rearrangement of the N- and C-terminal domains. In NarL, residue 204 faces the interdomain interface, and R1 is nearly completely immobilized relative to the protein and inaccessible to collision with Ni(EDDA). Phosphorylation triggers the appearance of a population of spin that is similar to R1 at a solvent-exposed helix surface site (196R1 or 211R1, for example). Moreover, the collision parameter for Ni(EDDA) has increased 4-fold to $\Pi = 0.2$, a value compatible with a helix surface site. These results can only be accounted for by a change that modulates the interdomain interface to expose 204R1 to solvent.

In this study, phosphorylation of NarL is produced by reaction of D59 with acetyl phosphate. It is possible that the changes in R1 reported above, in particular that at 204R1, result from reaction of acetyl phosphate at sites other than D59. To explore this possibility, the double mutant D59N/V204C was prepared and spin-labeled. The EPR spectrum was indistinguishable from that of D59/204R1 (data not shown). After a standard incubation of D59N/204R1 with acetyl phosphate, the EPR spectrum and molecular weight (determined by electrospray ionization mass spectrometry) of the double mutant were unchanged compared to the protein before acetyl phosphate reaction (data not shown). This confirms that D59 is the only site of reaction for acetyl phosphate and that the changes in EPR spectra result exclusively from phosphorylation of D59. The yield of the phosphorylation reaction for NarL was typically 80−90% as determined by nondenaturing PAGE.

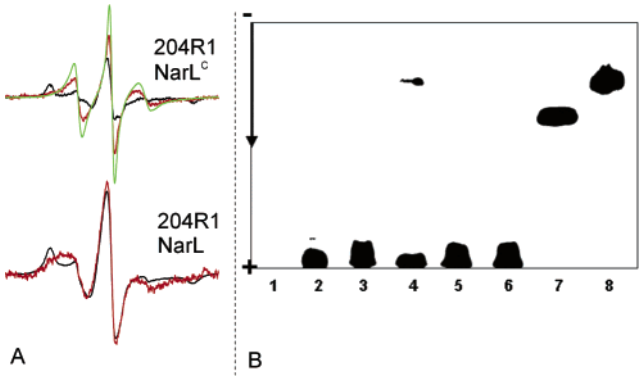

FIGURE 4: Linker-independent association of NarL^C with NarL^N. (A) EPR spectra of the C-terminal domain mutant 204R1. Top panel: isolated C-terminal domain 204R1 NarL^C (24 μM) mixed with excess NarL^N (96 μM) before (black trace) and after (red trace) phosphorylation of NarL^N. Also shown is the spectrum of NarL^C 204R1 alone (green trace). Bottom panel: full-length 204R1 NarL before (black trace) and after (red trace) phosphorylation (data reproduced from Figure 3). The scan width was 100 G, and the spectra were normalized to the same number of spins within each group. (B) Association of the two NarL domains assayed by electrophoresis on a 20% w/v acrylamide native PAGE gel (Phast System, Pharmacia). NarL^N and Narl^C were at a concentration of 58 μM for all lanes, and lanes with NarL^N and Narl^C mixtures had a molar ratio of 1:1. The arrow indicates the direction of migration. Lanes: 1, NarL^C; 2, NarL^N; 3, NarL^N phosphorylated; 4, NarL^C + NarL^N; 5, NarL^C + NarL^N mixed and then phosphorylated; 6, NarL^C + NarL^N phosphorylated; 7, NarL full length; 8, NarL full length phosphorylated.

Collectively, the data suggest that phosphorylation at D59 triggers a conformational change in NarL that preserves the basic integrity of the C-terminal domain but removes constraints on both the mobility and accessibility of 204R1 in the interdomain interface. To examine this important result in more detail, additional experiments were carried out. The N-terminal domain and the C-terminal domain carrying the mutation V204C were expressed separately, and the latter was spin-labeled to give 204R1. The EPR spectrum of the isolated and spin-labeled C-terminal domain (NarL^C) is shown in Figure 4A (green trace, upper panel). Unlike the situation in full-length NarL, the narrow line widths and overall spectral breadth indicate that R1 has high mobility, characteristic of a side chain on a solvent-exposed surface. Upon addition of an excess of the isolated N-terminal domain (NarL^N), the mobility of 204R1 is dramatically reduced, giving rise to a spectral line shape similar to that of the intact molecule (Figure 4A, black trace, upper panel; compare with bottom panel, black trace). This clearly demonstrates the formation of a complex between the N- and C-terminal domains with 204R1 at the interface, as in the native molecule. Moreover, addition of phosphorylated NarL^N to the spin-labeled NarL^C produces little change in the spectrum of NarL^C 204R1, demonstrating that phosphorylated NarL^N has a weak affinity for the surface of NarL^C bearing 204R1 (Figure 4A, red trace, top panel). NarL^C has a molecular weight roughly one-half that of NarL. Therefore, the spectral differences between NarL^C and whole NarL, and the changes observed due to complex formation, have a contribution from differences in rotational correlation time of the protein. However, this effect is far too small to account for the magnitude of changes observed.

The formation of a 1:1 complex between the isolated NarL^N and NarL^C domains, but not between NarL^C and the phosphorylated NarL^N domain, is directly demonstrated by the nondenaturing PAGE data in Figure 4B. The isolated NarL^C domain is highly positively charged and does not enter the gel, which is loaded at negative pole (lane 1). The isolated NarL^N domain (lane 2) and its phosphorylated analogue (lane 3) each run the full length of the gel. A mixture of the NarL^C and NarL^N domains (lane 4) clearly shows the presence of a component that runs at the position of the phosphorylated whole NarL (lane 8). The slower migration of the mixed component compared to full-length NarL (lane 7) is due to the presence of an extra His tag, which is present on both the isolated N-terminal and the isolated C-terminal domains. Phosphorylation of the NarL^N and NarL^C mixture (lane 5) or phosphorylation of the NarL^N domain before mixing with the NarL^C domain (lane 6) blocks the formation of the complex. Thus, domain association does not require the presence of the 18 amino acid linker, and specific interface interactions must exist to guide association of the isolated domains.

Phosphorylation-Induced Changes in the NarL Structure: Deductions from Changes in Interresidue Distances. Another strategy designed to examine phosphorylation-induced domain separation was direct distance measurement between two R1 residues, with one in each domain. This technique has been successfully applied for examining interdomain movements in T4 lysozyme and maltose-binding protein (*37*, *38*). Dipole−dipole interactions between R1 residues can be analyzed in terms of interspin distance, up to about 20 Å at room temperature (*27*, *39*).

The three NarL double mutants shown in Figure 5A were prepared for this purpose (78R1/196R1, 127R1/175R1, 132R1/211R1). Each pair was selected to monitor the relative positions of the N- and C-terminal domains near the interface. In the unphosphorylated state, the distances between the corresponding α-carbon atoms of the pairs in the crystal structure were in the range 7−11 Å, as indicated in Figure 5A, left panel. For residues with α-carbon distances in this range, measurable dipolar interactions between the nitroxides are anticipated (*27*).

A magnetic dipolar interaction between nitroxides leads to spectral broadening and a concomitant decrease in spectral amplitude. Thus, dipolar interactions can be recognized by the reduction in spectral amplitude of the doubly labeled mutant compared with that of a hypothetical noninteracting spectrum calculated as the algebraic sum of the corresponding single mutants (*27*). The EPR spectra of the three double mutants are shown as black traces in Figure 5B and those computed as the sum of the corresponding singly labeled mutants as superposed green traces. In each case, the amplitude difference between these spectra reveals a magnetic dipolar interaction, strongest for S78R1/K196R1 and E127R1/M175R1. Figure 5C shows the distributions of interspin distances in the three pairs of double mutants (black bars), as estimated from spectral simulations (*27*). The distances are consistent with the crystal structure of NarL and the known conformations of the R1 side chain (*27*, *31*).

When NarL is phosphorylated on residue D59 in the N-terminal domain, there is a dramatic *decrease* in the dipole−dipole interaction between 78R1 and 196R1, shown by the large increase in spectral amplitude (Figure

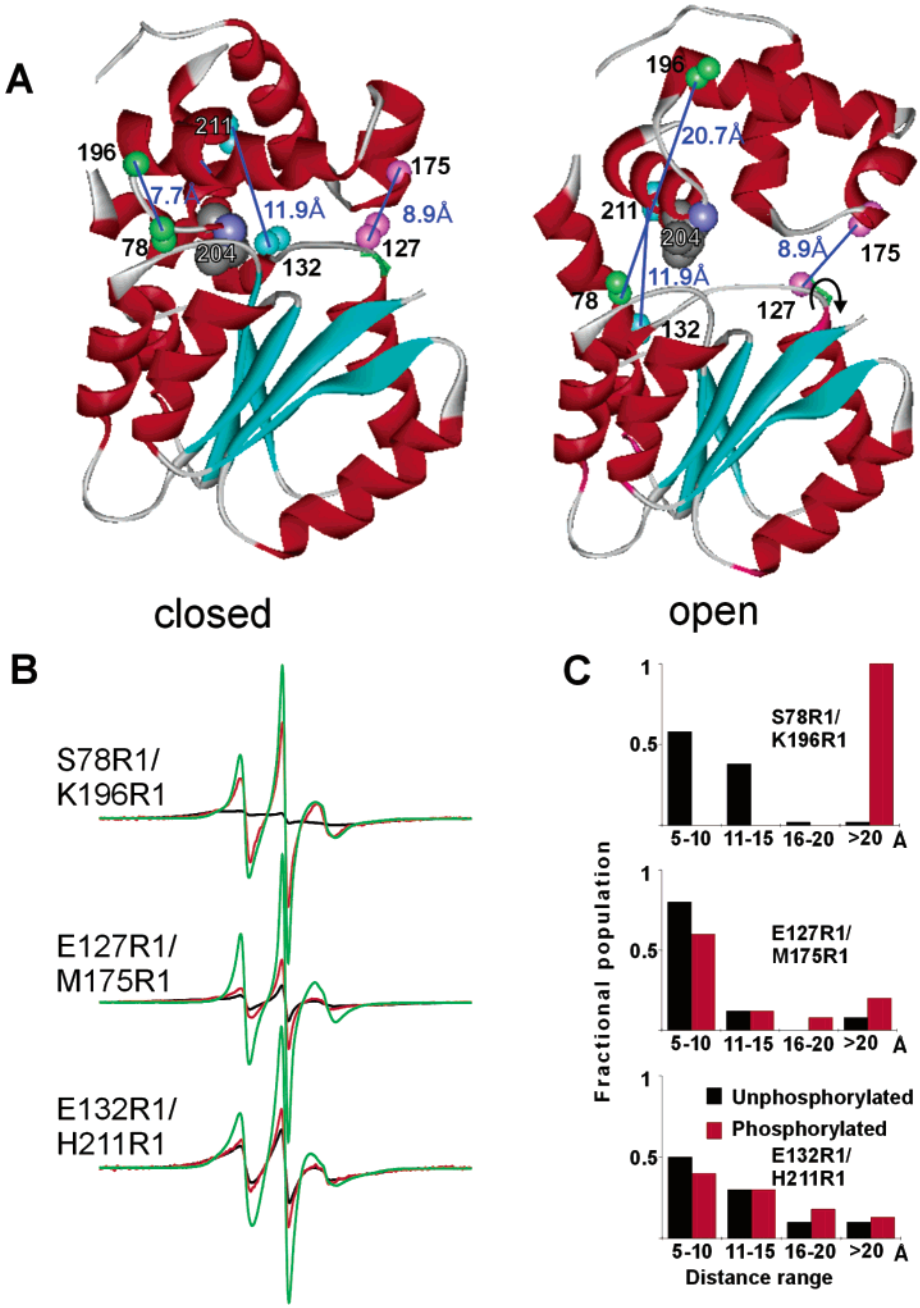

FIGURE 5: Models of NarL showing the location of double mutants and the corresponding EPR spectra. (A) Left panel: Ribbon model of NarL in the unphosphorylated state (*10*). The C_α and C_β atoms of the cysteine mutants are shown (same color spheres indicate respective pairs). Distances between the C_α atoms of each pair are indicated. A space-filling model of 204R1 is also shown. Right panel: Ribbon model for the phosphorylated state of NarL generated by rotation about the main chain dihedrals of G126 (indicated by arrow). The distances between C_α atoms are indicated. (B) EPR spectra for each mutant pair, including the spectrum of the unphosphorylated NarL (black trace), phosphorylated NarL (red trace), and the sum of the spectra of the corresponding singly labeled proteins (green trace). All spectra were recorded with a 150 G scan width and normalized to the same number of spins. (C) Estimated inter-nitroxide distance distributions for each double mutant (*27*) are shown in the bar graphs (black for unphosphorylated, red for phosphorylated).

5B, top panel, red trace) relative to the unphosphorylated state (Figure 5B, top panel, black trace). In fact, the spectrum in the phosphorylated state approaches that representing the noninteracting state (Figure 5B, top panel, green trace). This change is reflected in the distance distribution after phosphorylation, where essentially 100% of the population has a distance of 20 Å or greater, the limit of detection (Figure 5C, top panel, red bar).

On the other hand, there is relatively little change in distance between spins in 127R1/175R1 and 132R1/211R1 (Figure 5B,C, center and bottom panels). A model to account for the changes in both mobility of single R1 residues and the distance changes will be discussed below.

DISCUSSION

The data presented above lead to the remarkable conclusion that phosphorylation at site D59 in the N-terminal domain of NarL produces changes in structure detected by R1 side chains at multiple sites in the C-terminal domain, some of which are 40 Å distant from D59. However, the structural changes within the C-terminal domain likely reflect a small, localized conformational change rather than a global

change in the tertiary fold of the domain. This is suggested by the fact that R1 sensors at sites 196 and 211 in α9 and α10, respectively, detect no phosphorylation-dependent changes. In addition, the double mutants 127R1/175R1 and 132R1/211R1 involve residues in α8 and α9, respectively, and no change in interspin distances is sensed upon phosphorylation. These results make it unlikely that significant relative motions involving α8, α9, or α10 are triggered by phosphorylation. Finally, the recent crystal structure of the C-terminal domain bound to DNA shows the fold of the domain to be conserved in the bound state (*18*).

On the other hand, nitroxide sensors 161R1 and 169R1 in α7 and 157R1 and 171R1 in the interhelical loops at either end of this helix do experience notable changes in mobility, suggesting a motion of α7. One model to account for the essentially identical reductions in mobility of 161R1 and 169R1 upon phosphorylation is a small rigid body rotation of α7 about its axis, a motion that would bring the nitroxides into interaction distance with residues from α9. Changes in the interhelical loop residues 157R1 and 171R1 would accompany the motion of α7.

The most informative changes regarding the mechanism of activation by phosphorylation are the increase in mobility and accessibility of 204R1, a residue buried at the contact surface between the N- and C-terminal domains, and the dramatic change in distance between the R1 residues in the pair 78R1/196R1. The highly mobile and accessible state of 204R1 in the phosphorylated protein is incompatible with the N- and C-terminal domains remaining in contact at the surface found in the crystal structure. This result and the ≥10 Å increase in distance between 78R1/196R1 can be accounted for by a "closed" to "open" transition wherein the two domains separate by rotation about a hinge site (or sites). The hinge site must be located downstream of residue 127, because the 127R1/175R1 and 132R1/211R1 distances remain unchanged (sequence numbers above 126 are part of the C-terminal domain). Glycine 126 is a candidate hinge site, and for example Figure 5A, right panel, shows one model of phosphorylated NarL (open state) generated by rotation about the backbone dihedrals of G126 to produce a separation of ≈12 Å between 78R1/196R1. Within the context of this model, the α6 helix must be included as part of the C-terminal domain.

It should be emphasized that the EPR data show only that the majority of spin pairs separate beyond the range of detection (≥20 Å), so that the data are consistent with a spectrum of possible configurations that satisfy this constraint. Within the context of the hinge-bending model, it is likely that the hinge is flexible, and the structure fluctuates in time. Also shown in the figure is a space-filling model of V204, showing that the same G126 rotations that lead to internal consistency with the distance constraints also nicely account for the limited increase in the solvent accessibility of 204R1.

Are the closed and open conformations in equilibrium? In the unphosphorylated state, the EPR spectrum of the double mutant 78R1/196R1 shows no evidence of a second protein population with an interspin distance of ≥20 Å that would correspond to the open conformation. Even a few percent of such a population with sharp spectral features would be easily detected in the presence of the extremely broad spectrum of the closed state (Figure 5). Thus, there is a single conformation of unphosphorylated NarL in solution, and there is no detectable equilibrium between the closed and open conformations.

On the other hand, in the phosphorylated state, the spectrum of 204R1 has intensity in the region of the spectrum corresponding to an immobilized state, although it is not the major population. This could correspond to an equilibrium in which the structure fluctuates between the closed and open conformations. In the phosphorylated double mutant 78R1/196R1 with narrow spectral features, it would be difficult to detect a minor contribution of a strongly interacting (broad) population corresponding to the unphosphorylated protein. Thus, the data are not definitive but would be consistent with a "closed ↔ open" equilibrium in the phosphorylated state.

The data presented above provide structural evidence for a model of phosphorylation-triggered activation in regulator proteins of two-component regulatory systems. In this model, phosphorylation in the N-terminal domain triggers a global conformational change within the domain that weakens interactions at the interdomain interface. This in turn results in a separation of the two domains by rotation about a hinge that exposes critical DNA binding elements in the C-terminal domain. The present model draws support from other recent studies. First, studies on FixJ, NtrC, and SpoOA have shown that phosphorylation of the N-terminal domain of a response regulator does in fact induce global conformational changes that could modulate an interdomain interface (*14*−*17*). Phosporylation of CheB causes an increase in solvent accessibility of regions containing interdomain residues (*40*). Most importantly, the crystal structure of the $NarL^C$/DNA complex identifies α9 as the key DNA binding element (*18*), and motion of the N-terminal domain of the kind shown in Figure 5A exposes this helix for proper docking to DNA. Moreover, the $NarL^C$ is bound to DNA as a dimer in which V204 is a key residue at the new dimer interface. The data presented above show that phosphorylation triggers exposure of this previously buried site, an essential step in preparing the molecule for dimer formation in the DNA binding site.

ACKNOWLEDGMENT

We thank Gail Katsir for helpful discussions and assistance in phosphorylating NarL, Yandong Zhao and Michael R. Jarvis for assistance in NarL mutagenesis, Christian Altenbach for assistance in spectral simulations for distance determination, and Kym Faull and Julian Whitelegge of the UCLA Mass Spectrometry Facility for molecular weight determination of NarL and its derivatives.

REFERENCES

1. Parkinson, J. S., and Kofoid, E. C. (1992) *Annu. Rev. Genet. 26*, 71−112.
2. Hoch, J. A., and Silhavy, T. J., Eds. (1995) *Two Component Signal Transduction*, American Society of Microbiology, Washington, DC.
3. Stewart, V., and Rabin, R. S. (1995) in *Two Component Signal Transduction* (Hoch, J. A., and Silhavy, T. J., Eds.) pp 233−253, American Society of Microbiology, Washington, DC.
4. Lee, S.-Y., Cho, H. S., Pelton, J. G., Yan, D., Henderson, R. K., King, D. S., Huang, L.-S., Kustu, S., Berry, E. A., and Wemmer, D. E. (2001) *Nat. Struct. Biol. 8*, 52−56.
5. Lewis, R. J., Krzywda, S., Brannigan, J. A., Turkenburg, J. P., Muchova, K., Dodson, E. J., Barak, I., and Wilkinson, A. J. (2000) *Mol. Microbiol. 38*, 198−212.

6. Kern, D., Volkman, B. F., Luginbühl, P., Nohaile, M. J., Kustu, S., and Wemmer, D. E. (1999) *Nature 402*, 894−898.
7. Birck, C., Mourey, L., Gouet, P., Fabry, B., Schumacher, J., Rousseau, P., Kahn, D., and Samama, J.-P. (1999) *Struct. Folding Des. 7*, 1505−1515.
8. Solà, M., Gomis-Rüth, F. X., Serrano, L., González, A., and Coll, M. (1999) *J. Mol. Biol. 285*, 675−687.
9. Djordjevic, S., Goudreau, P. N., Xu, Q., Stock, A. M., and West, A. H. (1998) *Proc. Natl. Acad. Sci. U.S.A. 95*, 1381−1386.
10. Baikalov, I., Schroeder, I., Kaczor-Greskowiak, M., Greslowiak, K., Gunsalus, R. P., and Dickerson, R. E. (1996) *Biochemistry 35*, 11053−11061.
11. Baikalov, I., Schroeder, I., Kaczor-Greskowiak, M., Cascio, D., Gunsalus, R. P., and Dickerson, R. E. (1998) *Biochemistry 37*, 3665−3676.
12. Buckler, D. R., Zhou, Y., and Stock, A. M. (2002) *Structure 10*, 153−164.
13. Schröder, I., Wolin, C. D., Cavicchioli, R., and Gunsalus, R. P. (1994) *J. Bacteriol. 176*, 4985−4992.
14. Volkman, B. F., Lipson, D., Wemmer, D. E., and Kern, D. (2001) *Science 291*, 2429−2433.
15. Birck, C., Mourey, L., Gouet, P., Fabry, B., Schumacher, J., Rousseau, Kahn, D., and Samama, J.-P. (1999) *Structure 7*, 1505−1515.
16. Lewis, R. J., Brannigan, J. A., Katarína, M., Barák, I., and Wilkinson, A. J. (1999) *J. Mol. Biol. 294*, 9−15.
17. Hwang, I., Thorgeirsson, T., Lee, J., Kustu, S., and Shin, Y.-K. (1999) *Proc. Natl. Acad. Sci. U.S.A. 96*, 4880−4885.
18. Maris, A. E., Sawaya, M. R., Kaczor-Grzeskowiak, M., Jarvis, M. R. Bearson, S., Kopka, M. L., Schroeder, I., Gunsalus, R. P., and Dickerson, R. E. (2002) *Nat. Struct. Biol. 9*, 771−778.
19. Xiao, G., Cole, D. L., Gunsalus, R. P., Sigman, D. S., and Chen, C. B. (2002) *Protein Sci. 11*, 2427−2436.
20. Hubbell, W. L., Mchaourab, H. S., Altenbach, C., and Lietzow, M. A. (1996) *Structure 4*, 779−783.
21. Hubbell, W. L., Gross, A., Langen, R., and Lietzow, M. A. (1998) *Curr. Opin. Struct. Biol. 8*, 649−656.
22. Hubbell, W. L., Cafiso, D. S., and Altenbach, C. (2000) *Nat. Struct. Biol. 7*, 735−739.
23. Feix, J. B., and Klug, C. S. (1998) in *Biological Magnetic Resonance* (Berliner, L. J., Ed.) Vol. 14, pp 251−281, Plenum Press, New York.
24. Sambrook, J., Fritsch, E. F., and Maniatis, T. (1989) *Molecular Cloning*: *A Laboratory Manual*, 2nd ed., pp 15.74−15.79, Cold Spring Harbor Laboratory Press, Cold Spring Harbor, NY.
25. Altenbach, C., Greenhalgh, D. A., Khorana, H. G., and Hubbell, W. L. (1994) *Proc. Natl. Acad. Sci. U.S.A. 91*, 1667−1671.
26. Oh, K. J., Altenbach, C. Collier, R. J., and Hubbell, W. L. (2000) in *Methods in Molecular Biology. Vol. 145: Bacterial Toxins: Methods and Protocols* (Holst, O., Ed.) pp 147−169, Humana Press, Totowa, NJ.
27. Altenbach, C., Oh, K. J., Trabanino, R., Hideg, K., and Hubbell, W. L. (2001) *Biochemistry 40*, 15471−15482.
28. Whitelegge, J. P., Gundersen, C., and Faull, K. F. (1998) *Protein Sci. 7*, 1423−1430.
29. Isas, J. M., Langen, R., Haigler, H. T., and Hubbell, W. L. (2002) *Biochemistry 41*, 1464−1473.
30. Columbus, L., and Hubbell, W. L. (2002) *Trends Biochem. Sci. 27*, 288−295.
31. Langen, R., Oh, K. J., Cascio, D., and Hubbell, W. L. (2000) *Biochemistry 39*, 8396−8405.
32. Mchaourab, H. S., Lietzow, M. A., Hideg, K., and Hubbell, W. L. (1996) *Biochemistry 35*, 7692−7704.
33. Columbus, L., Kalai, T., Jeko, J., Hideg, K., and Hubbell, W. L. (2001) *Biochemistry 40*, 3828−3846.
34. Oh, K. J., Zhan, H., Cui, C., Hideg, K., Collier, R. J., and Hubbell, W. L. (1996) *Science 273*, 810−812.
35. Salwinski, L., and Hubbell, W. L. (1999) *Protein Sci. 8*, 562−572.
36. Hubbell, W. L., and McConnell (1971) *J. Am. Chem. Soc. 93*, 314−326.
37. Mchaourab, H. S., Oh, K. J., Fang, C. J., and Hubbell, W. L. (1997) *Biochemistry 36*, 307−316.
38. Hall, J. A., Thorgeirsson, T. E., Liu, J. Shin, Y.-K., and Nikaido, H. (1997) *J. Biol. Chem. 272*, 17610−17614.
39. Rabenstein, M. D., and Shin, Y.-K. (1995) *Proc. Natl. Acad. Sci. U.S.A. 92*, 8239−8243.
40. Hughes, C. A., Mandell, J. G., and, G. S., Stock, A. M., and Komives, E. A. (2001) *J. Mol. Biol. 307*, 967−976.

BI0272205